ACS Catalysis

Research Article

pubs.acs.org/acscatalysis

Promotion Effects of Nitrogen Doping into Carbon Nanotubes on Supported Iron Fischer–Tropsch Catalysts for Lower Olefins

Jinzhao Lu,[†] Lijun Yang,[†] Bolian Xu,*[,†] Qiang Wu,[†] Dong Zhang,[‡] Shijun Yuan,[‡] Ya Zhai,[‡] Xizhang Wang,*[,†] Yining Fan,[†] and Zheng Hu*[,†]

[†]Key Laboratory of Mesoscopic Chemistry of the Ministry of Education and Jiangsu Provincial Lab for Nanotechnology, Institute of Theoretical and Computational Chemistry, School of Chemistry and Chemical Engineering, Nanjing University, Nanjing 210093, China

[‡]Department of Physics, Southeast University, Nanjing 210096, China

Supporting Information

ABSTRACT: Fischer–Tropsch synthesis (FTS) is a classical topic of great significance because of the approach of post-petroleum times. For decades, people have attempted to develop iron-based FTS catalysts with high selectivity for lower olefins. By means of the anchoring effect and the intrinsic basicity of nitrogen-doped carbon nanotubes (NCNTs), iron nanoparticles were conveniently immobilized on NCNTs without surface premodification. The so-constructed Fe/NCNTs catalyst presents superb catalytic performance in FTS with high selectivity for lower olefins of up to 46.7% as well as high activity and stability. The excellent performance is well-correlated with enhanced dissociative CO adsorption, inhibition of secondary hydrogenation of lower olefins, and promoted formation of the active phase of χ-Fe_5C_2. All of these merits result from participation of the nitrogen, as revealed by our experimental characterization. These results may lead to a new strategy for exploring advanced FTS catalysts with abundant N-doped carbon nanostructures.

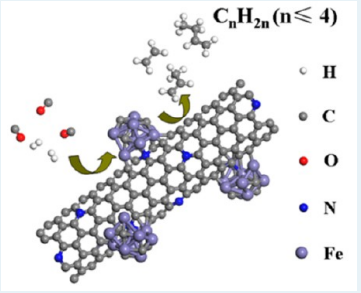

KEYWORDS: *nitrogen-doped carbon nanotubes, iron nanoparticles, heterogeneous catalysis, Fischer–Tropsch synthesis, basicity, lower-olefin selectivity*

1. INTRODUCTION

Lower olefins ($C_2^=$–$C_4^=$) are basic building blocks for petrochemicals with wide applications, which are usually produced by thermal or catalytic cracking of naphtha or vacuum gas oil.[1] With the rapid depletion of oil sources, Fischer–Tropsch synthesis (FTS) from synthesis gas (CO + H_2), which can be derived from natural gas, coal, or biomass, has become a sustainable strategy of great significance to produce various valuable chemicals.[2−6] For several decades, people have attempted to develop iron-based catalysts to direct the product selectivity of the FTS toward the high production of lower olefins.[6−15] However, the products in FTS usually follow the Anderson–Schulz–Flory (ASF) distribution, which imposes a limitation on the lower-olefin selectivity.[5,6] Extensive efforts have been devoted to enhance the lower-olefin selectivity by regulating the active species and catalyst support,[7−10] adding promoters[12−14] and optimizing the reaction conditions.[15] As is known, the catalyst support can significantly influence the catalytic performance mainly by its surface acidity/basicity and the metal–support interaction. These factors dominate the adsorption/desorption of the reactants/products,[16,17] the dispersion of the active phase,[18,19] the reduction and carbonization of the catalysts,[20,21] and consequently the catalytic activity and selectivity. Early studies found that the basic support of MgO was favorable to improve the selectivity for lower olefins.[22,23] However, the poor stability toward water and the relatively low surface area of MgO limits its application in FTS. In practice, bases of alkali metal ions are usually added to the iron catalysts as promoters to enhance the surface basicity, thereby reducing methane formation and improving the lower-olefin selectivity.[5,6] However, alkali promoters usually suffer from gradual loss during operation, especially in the case of water formation.[24]

In recent years, carbon nanotubes (CNTs) and carbon nanofibers (CNFs) have attracted increasing attention as new carbon supports because of their unique nanostructures and excellent properties such as large surface area, good thermal and chemical stability, and high electrical conductivity.[25] For many reactions, catalysts with CNTs/CNFs as the support demonstrate higher activity and selectivity than their counterparts with common supports such as activated carbon (AC), Al_2O_3, and SiO_2.[25] The catalytically active species could be selectively immobilized either on the external surface[8,9,25] or inside the nanospace of CNTs with the confinement effect.[11,14] In both cases, premodifications such as strong acid oxidation or cutting of the nanotube are required because of the inert nature of CNTs/CNFs, which are somewhat complex and may introduce contaminants and even impair the properties of the

Received: October 16, 2013
Revised: January 1, 2014
Published: January 9, 2014

CNTs/CNFs used. As for FTS to give lower olefins, good selectivity with high activity has recently been obtained using a CNTs-confined Fe catalyst,[11] and the highest selectivity been obtained using CNFs-supported Fe nanoparticles promoted with sulfur plus sodium.[8] In our recent studies on electrocatalysts, we found that N-doped carbon nanotubes (NCNTs) can provide effective anchoring sites for convenient immobilization of highly dispersive metal nanoparticles without premodification.[26−28] Moreover, NCNTs are a kind of support with intrinsic basicity.[29,30] The anchoring effect and intrinsic basicity of NCNTs suggests their great potential for use in the construction of Fe-based catalysts for the high production of lower olefins in FTS.[31]

In this work, iron nanoparticles were conveniently immobilized on NCNTs without premodification, and the Fe/NCNTs catalysts thus obtained demonstrate superb catalytic selectivity, activity, and stability in FTS to give lower olefins, much better than the counterpart catalysts using CNTs and AC supports. The excellent performance is well-correlated with the support effects, including the intrinsic basicity of the NCNTs and the suitable metal−support interaction due to participation of the nitrogen, which opens a promising route for the development of advanced FTS catalysts for high production of lower olefins.

2. EXPERIMENTAL SECTION

2.1. Preparation of the Catalysts. NCNTs with a nitrogen content of 3−5% were synthesized by in situ chemical vapor deposition and purified as described in our previous papers.[28,32] NCNTs-supported iron catalysts (denoted as Fe/NCNTs) were prepared by the incipient wetness impregnation method.[33] Briefly, the predetermined amount of iron nitrate was dissolved in distilled water, and the amount of solution was equal to the total pore volume of the NCNTs sample. Then the solution was added dropwise to the NCNTs. After the impregnation step, the sample was dried at 80 °C under a vacuum desiccator, heat-treated at 400 °C in an Ar flow for 2 h, and then cooled to room temperature (RT). Fe/NCNTs catalysts with iron loadings of 2, 5, 8, 10, 12, and 15 wt % were prepared. To prepare potassium-promoted Fe/NCNTs (marked as Fe−K/NCNTs), a little potassium nitrate was added to the solution of iron nitrate during preparation with a loading of 0.5 wt %.

For comparison, iron species with a loading of 10 wt % were also supported on CNTs and AC by the same method. In this case, the CNTs or AC was pretreated in 7.5 mol L^{-1} nitric acid at 120 °C for 2 h, washed, and dried sequentially. The pretreated CNTs are simply denoted as t-CNTs and the untreated CNTs as u-CNTs in this study. The parameters of all the supports used are listed in Table 1.

2.2. Characterization. The surface area and pore volume of the supports were measured using an ASAP-2020 system from Micromeritics. The pore size distributions were estimated from the desorption branches of the N_2 isotherms using the Barrett−Joyner−Halenda (BJH) method. The morphologies and structures of the samples were observed by transmission electron microscopy (TEM) and high-resolution TEM (HRTEM) using a JEOL-JEM-2100 microscope operating at 200 kV.

The final compositions of the catalysts were examined by inductively coupled plasma mass spectrometry (ICP-MS). The catalysts were also characterized by X-ray diffraction (XRD) (Bruker AXS GmbH, D8 Advance A25 diffractometer equipped with a Co target, $\lambda_{K\alpha 1}$ = 0.178897 nm), X-ray photoelectron spectroscopy (XPS) (Thermo ESCALAB 250 spectrometer), Raman spectroscopy (Renishaw inVia Raman microscope with an argon-ion laser at an excitation wavelength of 514 nm), and Fourier transform infrared spectroscopy (FTIR) (Avatar 380 spectrometer). For the XRD patterns, 2θ was converted to the corresponding value for a Cu Kα1 source using MDI Jade software (version 6.5). Transmission ^{57}Fe Mössbauer spectra were collected at RT with a conventional constant-acceleration spectrometer using a ^{57}Co (Rh) source. The spectrometer was calibrated using an α-Fe foil. To prevent oxidation of the samples after reduction and reaction, the samples were first cooled to RT in nitrogen (purity of 99%) and then passivated for 1 h before exposure to air for characterization. The specimen for the Mössbauer measurement was further sealed in the holder with paraffin wax.

Temperature-programmed desorption (TPD) of CO_2, CO, and C_2H_4/C_3H_6 was carried out on a home-built four-channel reactor and monitored using an online quadruple mass spectrometer (AMETEK DYCOR Dymaxion 300MS, Balzer MID). Usually, 100 mg samples were used for measurements.

For CO_2 TPD of the NCNTs or t-CNTs support, the sample was pretreated at 150 °C in a He flow for 1 h to remove traces of water and impurities. Then CO_2 was adsorbed at RT for 1 h and subsequently purged with He for an additional 1 h until a stable baseline was achieved. The CO_2 TPD curve was recorded by MS (m/z 44 for CO_2) from RT to 800 °C at a heating rate of 10 °C min^{-1}. For contrast, the sample was also pretreated at 500 °C in a He flow for 1 h while keeping all the other procedures unchanged.

For CO TPD of the Fe/NCNTs or Fe/t-CNTs catalyst, the sample was reduced in a flow of H_2 at 380 °C for 12 h. Then CO was adsorbed at RT for 1 h and subsequently purged with He for an additional 1 h until a stable baseline was achieved. The CO TPD curve was recorded by MS (m/z 28 for CO) from RT to 800 °C at a heating rate of 10 °C min^{-1}.

For C_2H_4/C_3H_6 TPD of the Fe/NCNTs or Fe/t-CNTs catalyst after the reaction, the sample was treated at 300 °C in a He flow for 6 h to remove impurities. Then the C_2H_4/C_3H_6 gas mixture was adsorbed at RT for 1 h and subsequently purged with He for an additional 1 h until a stable baseline was achieved. The C_2H_4/C_3H_6 TPD curve was recorded by MS (m/z 26, 27, and 28 for C_2H_4 and m/z 27, 39, 41, and 42 for C_3H_6) from RT to 600 °C at a heating rate of 20 °C min^{-1}.

H_2 temperature-programmed reduction (TPR) was recorded using a gas chromatograph equipped with a thermal conductivity detector. 100 mg of catalyst was treated at 150 °C in an Ar flow for 1 h to remove traces of water and impurities and then cooled to RT. The gas mixture (5% H_2 + 95% Ar) flow was introduced to the catalyst bed until a stable baseline was reached. The H_2 TPR curve was recorded from RT to 800 °C at a heating rate of 10 °C min^{-1}.

2.3. Catalytic Tests. FTS reactions were conducted in a fixed-bed microreactor under atmospheric pressure. Typically, 100 mg of catalyst was charged into the quartz tube reactor. Before the reaction, the catalyst was reduced at 380 °C in H_2 for 12 h. Then the temperature was decreased to the designed reaction temperature (e.g., 300 °C), and syngas was fed into the reactor at a certain flow rate. The feed gas consisted of N_2 (10 vol %), CO (45 vol %), and H_2 (45 vol %). N_2 was used as an internal standard to ensure an accurate carbon balance. The exhaust was heated and introduced into a 10-way valve. All of the hydrocarbons were analyzed online using a gas chromato-

dx.doi.org/10.1021/cs400931z | ACS Catal. 2014, 4, 613−621

graph equipped with two capillary columns: C_1-C_4 hydrocarbons were analyzed with a PLOT-Al_2O_3 capillary column and C_{5+} hydrocarbons were analyzed with an HP-PONA capillary column. CO, CO_2, and CH_4 flowed through the cold trap and were analyzed using a thermal conductivity detector with a TDX-01 column. The hydrocarbon selectivity was calculated on a carbon basis.

3. RESULTS AND DISCUSSION

3.1. Support Characterization. Figure 1 shows typical TEM images of NCNTs and t-CNTs supports used in this study. Apparent morphological differences between the NCNTs and t-CNTs can be observed. NCNTs show straight, bamboo-like structures (Figure 1a,b) due to nitrogen incorporation, which are much different from the structures of t-CNTs (Figure 1c,d). Similar isotherms and pore size distributions were observed for NCNTs and t-CNTs (section SI-1 in the Supporting Information). The treatment of the u-CNTs in 7.5 mol L^{-1} nitric acid at 120 °C for 2 h increased the Brunauer–Emmett–Teller (BET) surface area and pore volume from 198 m^2 g^{-1} and 0.64 cm^3 g^{-1} for the u-CNTs to 285 m^2 g^{-1} and 0.70 cm^3 g^{-1} for the t-CNTs, respectively. The BET surface area and total pore volume of the NCNTs are a little smaller than the corresponding ones of t-CNTs (Table 1).

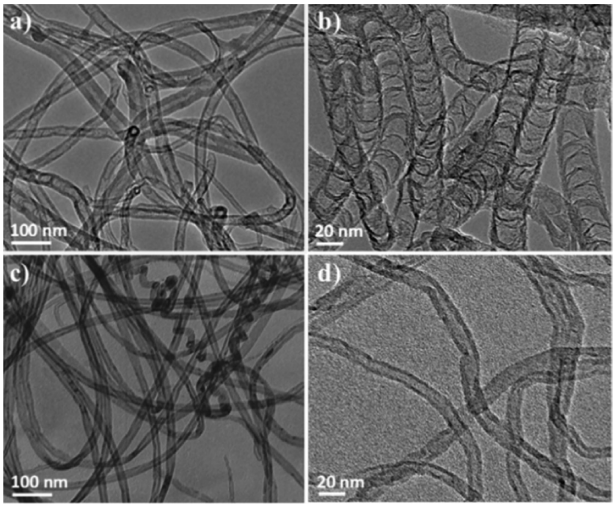

Figure 1. TEM images of (a, b) NCNTs and (c, d) t-CNTs at different magnifications.

FTIR was used to examine the surface functional groups of the NCNTs, u-CNTs, and t-CNTs (Figure 2). After the treatment in 7.5 mol L^{-1} nitric acid, new bands at 1714 and 1112 cm^{-1} appeared for the t-CNTs, which are assigned to the C=O vibration and C–O stretching of carboxylic groups, respectively.[34,35] The results verified that the HNO_3 treatment introduced carboxylic functions at the t-CNTs surface. By contrast, no carboxylic groups were detected in the NCNTs. Two identical peaks were observed at 1400 and 1630 cm^{-1} for NCNTs, u-CNTs, and t-CNTs. The band at 1400 cm^{-1} can be ascribed either to aromatic C=C bonds and various substitution modes of the aromatic ring or to carboxyl-carbonate structures,[36] and that at 1630 cm^{-1} is due to water absorption on the support.[34]

Table 1. Comparison of Some Parameters of the Different Carbon Supports

support	BET surface area (m^2 g^{-1})	external surface area (m^2 g^{-1})	total pore volume (cm^3 g^{-1})	micropore volume (cm^3 g^{-1})
AC	1307	916	0.77	0.26
u-CNTs	198	178	0.64	0.0072
t-CNTs	285	265	0.70	0.0073
NCNTs	235	216	0.44	0.0058

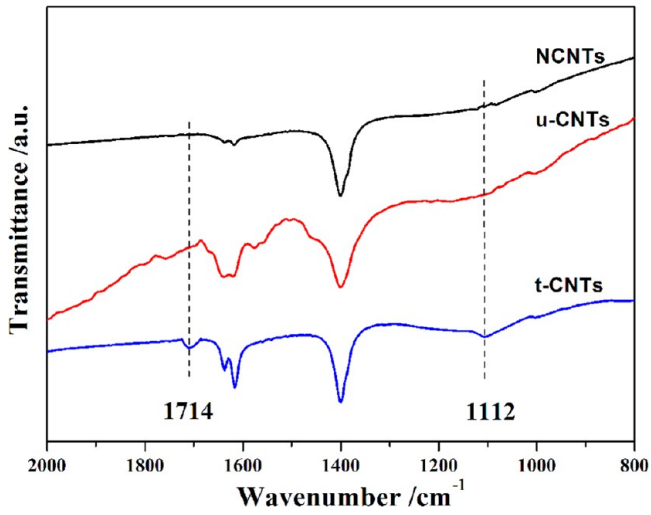

Figure 2. FTIR spectra of the NCNTs, u-CNTs and t-CNTs.

3.2. Catalyst Construction. Figure 3 shows typical TEM and HRTEM images of the catalysts activated by H_2 reduction (before FTS reaction). The iron species are homogeneously dispersed on the outer surfaces of the NCNTs without any surface pretreatment (Figure 3a,b). By contrast, pretreatment was required to immobilize iron species on t-CNTs (Figure 3c); otherwise, iron species could not be effectively dispersed (Figure 3d). The average particle size for Fe/NCNTs was 7–8 nm (Figure 3a,b), which is slightly smaller than that for Fe/t-CNTs (8–10 nm; Figure 3c).

XRD patterns of the catalysts are shown in Figure 4. The peaks at 26.3° and 43.8° are attributed to the (002) and (101) diffractions of the C-based supports. For all of the catalysts heat-treated at 400 °C in Ar (before H_2 reduction), the iron species exist as a mixture of Fe_2O_3 and Fe_3O_4 (Figure 4a, lines 1 and 2). After H_2 reduction, the diffraction peaks of the iron oxides at ~35° are greatly reduced, and new peaks appear at 44° and 65° that are attributed to (110) and (200) diffractions of Fe^0 (Figure 4a, lines 1′ and 2′). The weak peak at ~35° results from surface oxidation of the reduced iron particles during passivation and exposure to air. This result is in accordance with the HRTEM characterization (Figure 3b and section SI-2 in the Supporting Information). Figure 4b shows that as the Fe loading was increased from 2 to 15 wt %, the relative intensity of the diffractions from Fe_3O_4 gradually decreased while that from Fe_2O_3 gradually increased. Hence, Fe_3O_4 and Fe_2O_3 in Figure 4a are mainly attributed to the interfacial and bulk components, respectively. These results (Figures 3 and 4) indicate that because of the suitable interactions, N doping helps with the convenient high dispersion of the iron species but does not lead to the formation of compounds between the iron species and the NCNTs support. Such a situation is different from the cases for SiO_2 and Al_2O_3 supports, where harmful compounds such as

dx.doi.org/10.1021/cs400931z | ACS Catal. 2014, 4, 613–621

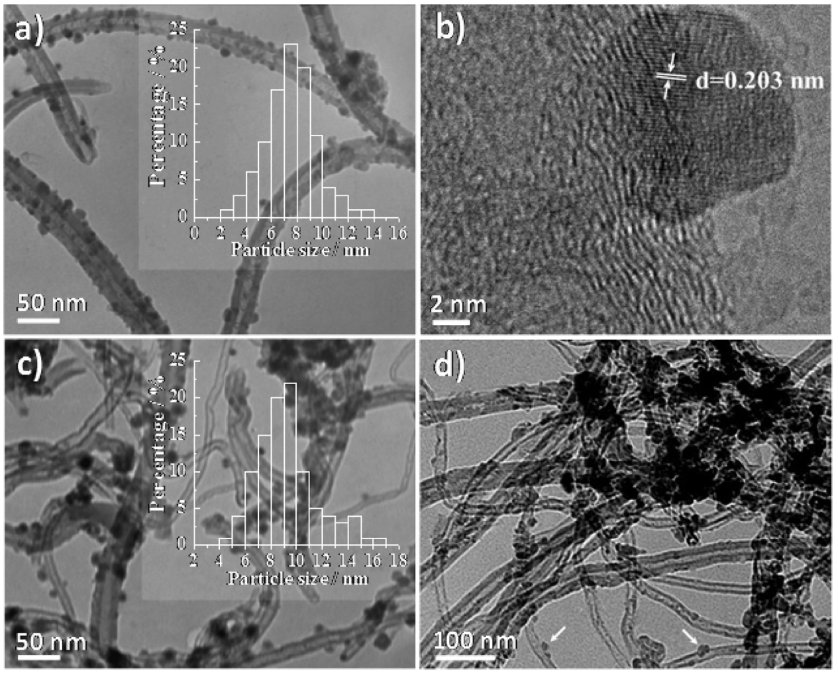

Figure 3. TEM and HRTEM images of activated catalysts with an Fe loading of 10 wt %: (a, b) Fe/NCNTs; (c) Fe/t-CNTs; (d) Fe/u-CNTs. The insets in (a) and (c) are the corresponding particle size distributions. The lattice distance of Fe (d_{110} = 0.203 nm) is discernible in (b). The Fe/u-CNTs sample shown in (d) was obtained by immobilizing Fe nanoparticles on u-CNTs for comparison with (c), and the aggregation is serious, although some dispersed iron particles are observable, as marked by the arrows.

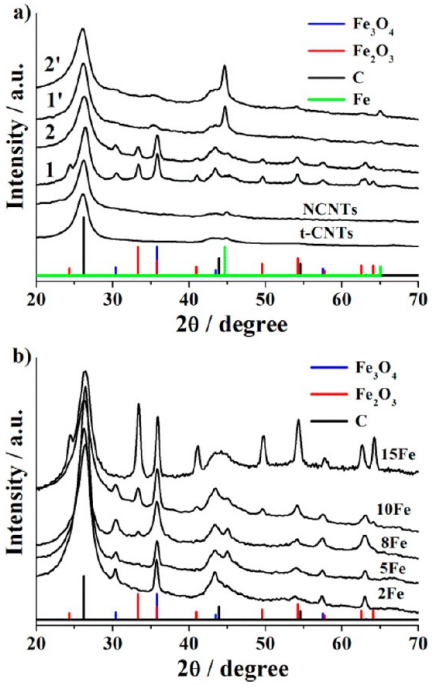

Figure 4. XRD patterns of the catalysts. (a) Fe/t-CNTs and Fe/NCNTs catalysts with Fe loadings of 10 wt %. XRD patterns of t-CNTs and NCNTs are also presented for reference. The patterns labeled 1 and 1′ are for the Fe/t-CNTs catalyst before and after H_2 reduction, respectively, and those labeled 2 and 2′ are for the Fe/NCNTs catalyst before and after H_2 reduction, respectively. Peaks for Fe_2O_3 (JCPDS no. 13-0534), Fe_3O_4 (JCPDS no. 75-0449), and Fe^0 (JCPDS no. 06-0696) are also shown. (b) The iron phase transformation for Fe/NCNTs as the Fe loading increases from 2 to 15 wt %.

Fe_2SiO_4 and $FeAlO_3$ are formed because the interactions between the iron species and the supports are too strong.[37,38]

XPS characterizations (Figure 5) were conducted to analyze the elemental composition as well as the chemical bonding environment of the iron atoms. As depicted in Figure 5b, the same two O 1s peaks at ~530.4 and ~531.6 eV, corresponding to oxide anion (O^{2-}) and adsorbed atomic oxygen ($O_{(ads)}$), were observed for Fe/t-CNTs, Fe/NCNTs, and Fe_2O_3.[39,40] The peak at ~532.3 eV for Fe/t-CNTs and Fe/NCNTs is attributed to the hydroxide anion (OH^-).[39] However, for Fe/t-CNTs, an extra peak appears at ~533.6 eV that is ascribed to carboxylic groups (COOH) introduced by the HNO_3 treatment.[41,42] The N 1s peaks for NCNTs and Fe/NCNTs at ~398.6, ~400.0, ~401.2, and >402 eV are ascribed to pyridinic, pyrrolic, and graphitic nitrogen and oxidized or molecular nitrogen, respectively (Figure 5c).[41] The Fe 2p peaks of Fe/t-CNTs and Fe/NCNTs appear at ~711 eV (Fe $2p_{3/2}$) and ~724 eV (Fe $2p_{1/2}$) with a shakeup satellite line at ~719 eV, which is characteristic of Fe^{3+} (Figure 5d).[40] Specifically, the Fe^{3+} $2p_{3/2}$ peaks of Fe/t-CNTs and Fe/NCNTs appear at 711.3 and 711.2 eV, respectively, which are a little higher in energy than the peak at 710.8 eV for Fe_2O_3. These results suggest the existence of a small amount of Fe_3O_4 species in Fe/t-CNTs and Fe/NCNTs, since the Fe^{3+} $2p_{3/2}$ peak for Fe_3O_4 at 711.4 eV is about 0.6 eV higher than that for Fe_2O_3 at 710.8 eV;[40] this is in agreement with the XRD characterization results shown in Figure 4a.

3.3. Catalytic Performance. The effect of iron loading on the CO conversion and $C_2^=-C_4^=$ selectivity for the Fe/NCNTs catalysts was evaluated at two flow rates, and the results are shown in Figure 6 and section SI-3 in the Supporting Information. The CO conversion and $C_2^=-C_4^=$ selectivity obviously increased as the iron loading increased from 2 to 10 wt % and then gradually decreased when the iron loading was greater than 10 wt %. Hence, the optimal Fe/NCNTs catalyst

dx.doi.org/10.1021/cs400931z | ACS Catal. 2014, 4, 613−621

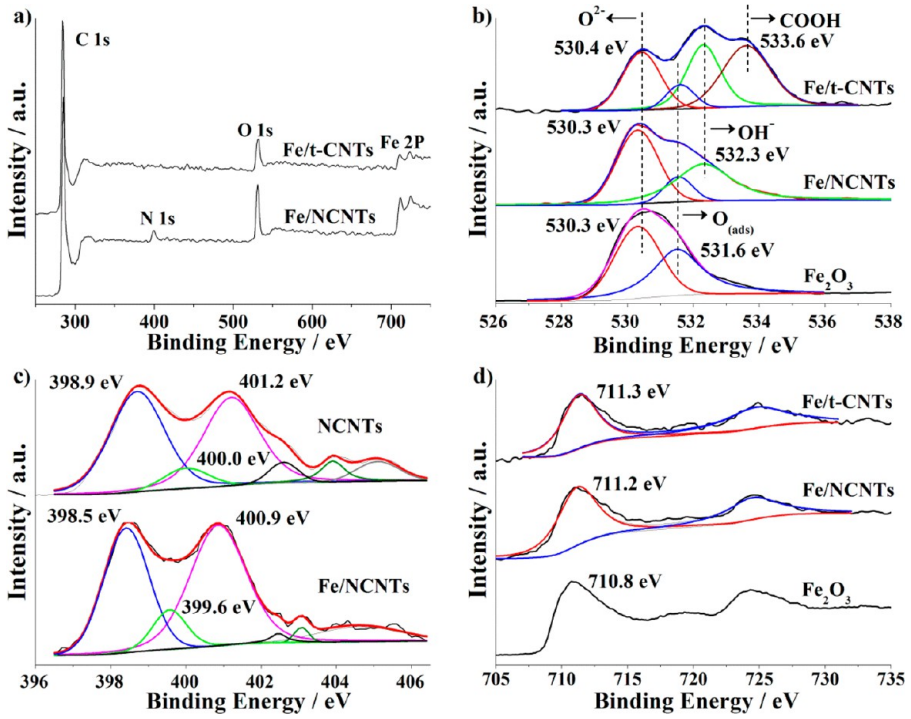

Figure 5. XPS spectra of the catalysts with an Fe loading of 10 wt %: (a) wide-survey spectra of Fe/t-CNTs and Fe/NCNTs; (b) O 1S spectra of Fe/t-CNTs, Fe/NCNTs and Fe_2O_3; (c) N 1S spectra of NCNTs and Fe/NCNTs; (d) Fe 2p spectra of Fe/t-CNTs, Fe/NCNTs, and Fe_2O_3. All of the binding energies are referenced to C 1s at 284.6 eV.

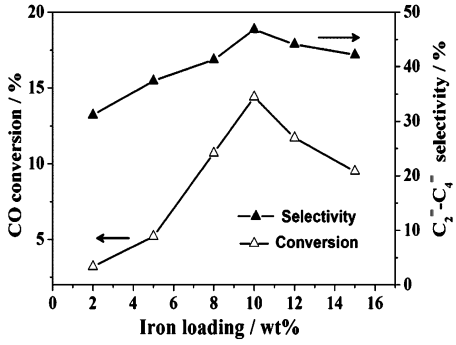

Figure 6. Effects of iron loading on the CO conversion and $C_2^=-C_4^=$ selectivity. Reaction conditions: 100 mg of catalyst, 300 °C, 1 bar, 4200 mL h^{-1} g^{-1}, H_2/CO = 1.

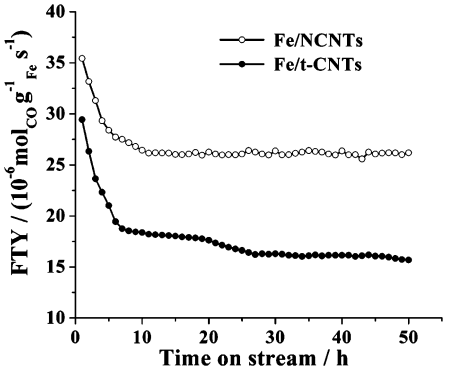

Figure 7. FTY as a function of time on stream for the Fe/NCNTs and Fe/t-CNTs catalysts. Reaction conditions: 300 °C, 1 bar, 4200 mL h^{-1} g^{-1}, H_2/CO = 1.

has an iron loading of 10 wt %. An iron loading of 10 wt % has often been used in the literature with t-CNTs or CNFs supports.[8,9,33,43] Thus, catalysts with an iron loading of 10 wt % were used in the subsequent experiments.

The Fe/NCNTs and Fe/t-CNTs catalysts were evaluated in FTS at 300 °C and 1 bar, as shown in Figure 7 and Table 2 (the catalyst compositions are shown in section SI-4 in the Supporting Information). The catalytic activity is expressed as iron time yield (FTY), which is the number of moles of CO converted to hydrocarbons per gram of iron per second. Both the initial and steady-state activities of Fe/NCNTs were much better than the corresponding ones for Fe/t-CNTs. A high initial activity was observed for the Fe/NCNTs catalyst, which decreased during the first 6 h on stream and then reached a steady state without detectable deterioration during our measurement over the following ca. 40 h. In contrast, the Fe/t-CNTs catalyst exhibited a lower initial activity, bigger decrement in the initial reaction period, and a lasting deactivation tendency.

Table 2 clearly indicates the effect of the support on the steady-state catalytic performance. Under the same conditions, the Fe/NCNTs catalyst exhibited the best catalytic performance among the three catalysts with different carbon supports in this study. Specifically, the FTY of Fe/NCNTs (26.5 μmol_{CO} g_{Fe}^{-1} s^{-1}) was about 1.6 times that for Fe/t-CNTs (16.2 μmol_{CO} g_{Fe}^{-1} s^{-1}), and 2.7 times that for Fe/AC (9.9 μmol_{CO} g_{Fe}^{-1} s^{-1}), and the lower-olefin selectivity of Fe/NCNTs reached as high as 46.7%, which is much better than those for Fe/t-CNTs (36.4%) and Fe/AC (30.6%). In addition, methane formation was suppressed for Fe/NCNTs in comparison to Fe/t-CNTs, which is highly desired for obtaining the maximum production of the lower-olefin fraction.[8,44] When a small amount of potassium as an alkali promoter was added to give the Fe−K/NCNTs catalyst, the catalytic performance was

dx.doi.org/10.1021/cs400931z | ACS Catal. 2014, 4, 613−621

Table 2. Effect of the Support on the Catalytic Performance[a]

catalyst	CO conversion (%)	FTY ($\mu mol_{CO}\ g_{Fe}^{-1}\ s^{-1}$)	CO_2 selectivity (mol %)	product distribution (%)			
				CH_4	$C_2^=-C_4^=$	$C_2^0-C_4^0$	C_{5+}
Fe/NCNTs	14.4	26.5	18.6	22.2	46.7	5.7	25.4
Fe/t-CNTs	9.1	16.2	16.8	30.6	36.4	7.8	25.2
Fe/AC	4.8	9.9	9.9	17.4	30.6	7.5	44.5
Fe−K/NCNTs	16.5	27.9	23.6	17.3	54.6	5.9	22.2

[a]Reaction conditions: 100 mg of catalyst, 300 °C, 1 bar, 4200 mL h^{-1} g^{-1}, H_2/CO = 1.

further improved, as expected (Table 2 and section SI-5 in the Supporting Information). The chain growth probability (α) was estimated to be 0.53 for Fe/NCNTs, 0.58 for Fe/t-CNTs, 0.66 for Fe/AC, and 0.50 for Fe−K/NCNTs, according to the respective Anderson−Schulz−Flory plots (Figure S5 in section SI-6 in the Supporting Information). As is known, the optimal value of α for maximum lower-olefin production is between 0.4 and 0.5.[6] Thus, the α value for Fe/NCNTs catalyst (0.53) is close to the optimal value. The Fe/NCNTs catalyst was also tested at a higher CO conversion level by increasing the temperature to 350 °C and the pressure to 5 bar, and a high selectivity for lower olefins was still observed (section SI-5 in the Supporting Information). Hence, in addition to the convenient construction, the Fe/NCNTs catalyst presents a general advantage from the viewpoint of high $C_2^=-C_4^=$ selectivity, high activity, and low CH_4 production. The suppressed methane formation for Fe/NCNTs is also supported by theoretical calculations (section SI-7 in the Supporting Information).

3.4. Promotion Effects of N Doping into Carbon Nanotubes. *3.4.1. Adsorption and Desorption.* The preceding experimental results indicate that N doping not only helps with the convenient immobilization of the iron species but also dramatically improves the catalytic performance by increasing the catalytic activity and lower-olefin production and reducing methane formation. This should be correlated with the unique properties of the NCNTs due to N doping. Thus, the intrinsic basicity of the NCNTs support and the adsorption/desorption of the probe molecules on the derived Fe/NCNTs catalyst were characterized by CO_2, CO, and C_3H_6 TPD, as shown in Figure 8. In Figure 8a, both the NCNTs and the preoxidized t-CNTs have a CO_2 TPD peak, located at 230 and 330 °C, respectively (lines 1 and 2). The difference is that after 500 °C treatment in He for 1 h, the desorption peak for NCNTs remains but the one for the preoxidized t-CNTs disappears (lines 1′ and 2′, respectively). These results indicate that the peak in line 1 comes from chemisorbed CO_2, which means that there are quite stable basic sites on the NCNTs due to N doping[29,30] that can at least endure 500 °C treatment in He for 1 h as reflected in line 1′. By contrast, the peak in line 2 is attributed to decomposition of the carboxyl groups on the preoxidized t-CNTs introduced by nitric acid treatment,[45] which can be removed by 500 °C treatment in He, as reflected in line 2′ and also supported by the FTIR characterization in Figure 2. As a control, the untreated CNTs (u-CNTs) present a negligible CO_2 TPD peak (line 3). The basicity of the NCNTs support is the favorable factor for the higher lower-olefin production, since it is beneficial for CO chemisorption (thereby suppressing H_2 adsorption)[5,14,46] and lower-olefin desorption (thereby suppressing their secondary hydrogenation)[5,16,22,23] on the corresponding Fe/NCNTs catalyst. These speculations were indeed confirmed in our experiments as demonstrated below.

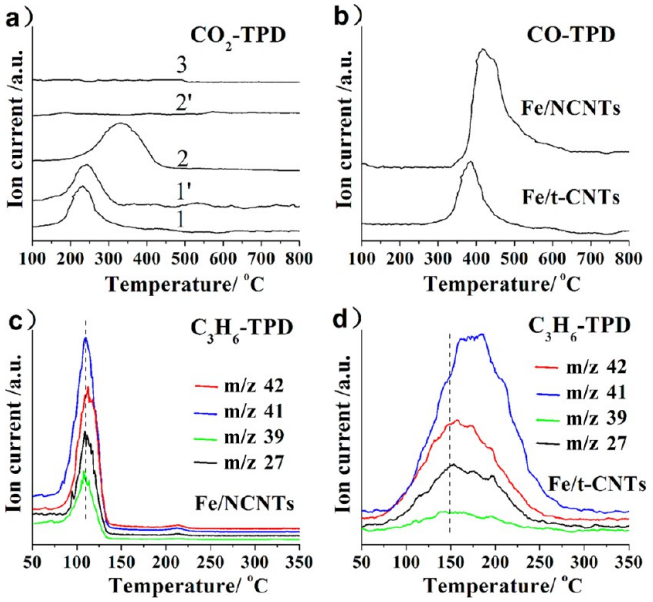

Figure 8. Characterization of the intrinsic basicities of the NCNTs and CNTs supports and adsorption/desorption of the probe molecules on the derived Fe/NCNTs and Fe/t-CNTs catalysts. (a) CO_2 TPD profiles of the supports: line 1, NCNTs; line 1′, NCNTs after 500 °C pretreatment in He for 1 h; line 2, preoxidized CNTs; line 2′, preoxidized CNTs after 500 °C pretreatment in He for 1 h; line 3, u-CNTs. (b) CO TPD profiles for the reduced Fe/NCNTs and reduced Fe/t-CNTs catalysts. (c, d) C_3H_6 TPD profiles for the used Fe/NCNTs and Fe/t-CNTs catalysts, respectively.

In the CO TPD profiles (Figure 8b), the reduced Fe/NCNTs catalyst presents a desorption peak at 420 °C (onset at ~330 °C), which is obviously higher than that at 384 °C (onset at ~280 °C) for the reduced Fe/t-CNTs catalyst. This result clearly indicates the stronger CO adsorption on Fe/NCNTs than on Fe/t-CNTs, which is attributed to the basicity of the NCNTs. Similar enhancements of CO chemisorption due to the increased surface basicity were observed on K- or Mn-promoted iron catalysts.[5,14,46] The electron transfer from nitrogen to the empty 3d orbital of iron,[47] as supported by our Raman characterization (section SI-8 in the Supporting Information), may increase the electron density of the iron species, which can strengthen the Fe−C bond and weaken the C−O bond.[5,46] The enhanced adsorption makes the CO dissociation the easier on Fe/NCNTs than on Fe/t-CNTs. In addition, in the C_3H_6 TPD profiles, the used Fe/NCNTs catalyst shows a C_3H_6 desorption peak at 112 °C, which is obviously lower than that at 156 °C for the used Fe/t-CNTs catalyst (Figure 8c,d). This result indicates the easier desorption of lower olefins from Fe/NCNTs, which favors the suppression of their secondary hydrogenation to alkanes, as expected.[5,16,22,23]

dx.doi.org/10.1021/cs400931z | ACS Catal. 2014, 4, 613−621

In a word, the basic NCNTs support contributes to the higher lower-olefin selectivity of the Fe/NCNTs catalyst by enhancing CO adsorption, suppressing H_2 adsorption, and promoting the desorption of lower olefins (section SI-9 in the Supporting Information).

3.4.2. Reduction and Carbonization. Recent progress indicates that the good reducibility of iron species and the resulting facile formation of the more active iron carbide phase are essential for obtaining high FTS activity.[48,49] Thus, we compared the reducibility and carbonization of Fe/NCNTs with Fe/t-CNTs by H_2 TPR, Mössbauer spectroscopy, and XRD, as shown in Figure 9. Both Fe/NCNTs and Fe/t-CNTs

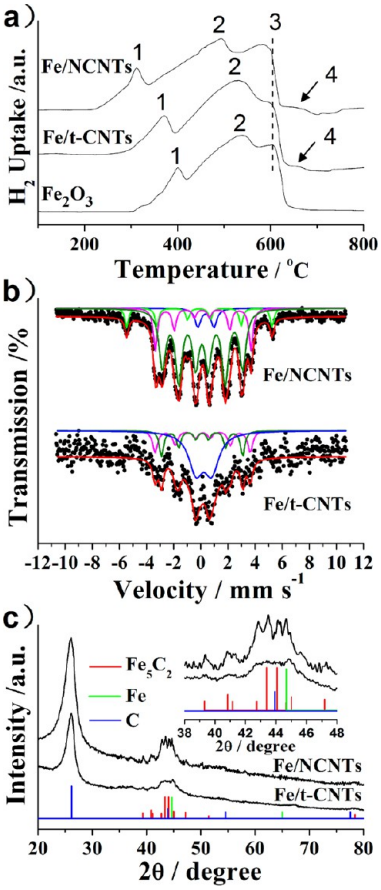

Figure 9. Comparison of the reducibility and carbonization of Fe/NCNTs with those of Fe/t-CNTs. (a) H_2 TPR profiles for the Fe/NCNTs and Fe/t-CNTs catalysts as well as Fe_2O_3 powder for reference. (b) Mössbauer spectra and (c) XRD patterns for the used Fe/NCNTs and Fe/t-CNTs catalysts, respectively. The inset in (c) is a local enlargement of the spectra for 2θ = 38−48°. Peaks for Fe_5C_2 (JCPDS no. 51-0997) and Fe^0 (JCPDS no. 06-0696) are referenced.

as well as Fe_2O_3 powder for reference present three reduction peaks below 650 °C in the H_2 TPR curves, marked as peaks 1−3, corresponding to the progressive reduction from Fe_2O_3 through Fe_3O_4 and FeO to Fe^0 (Figure 9a).[50] The trace peak 4 comes from gasification of the carbon-based support above ∼650 °C.[50] Compared with the case for Fe_2O_3, peaks 1−3 for Fe/NCNTs and Fe/t-CNTs both shift toward lower temperature, and this phenomenon is more obvious for Fe/NCNTs than Fe/t-CNTs. Specifically, peaks 1−3 for Fe/NCNTs are located at 313, 495, and 584 °C, about 57, 35, and 14 °C lower than the respective locations of 370, 530, and 598 °C for Fe/t-CNTs. This result indicates that both the NCNTs and t-CNTs supports can promote the reduction of iron oxide, and the effect is more obvious for NCNTs. Upon the introduction of syngas under the reaction conditions, the reduced iron is readily converted to a mixture of metal, carbides, and oxides, among which the iron carbides are generally essential for high FTS activity.[4,5,51−53] As revealed by the Mössbauer spectra, the used Fe/NCNTs catalyst generates much more χ-Fe_5C_2 than the used Fe/t-CNTs catalyst, as expected, with relative areas of 84.4 and 43.2%, respectively, in accordance with the clearer XRD profiles for the former (Figure 9b,c and Table 3). This result

Table 3. Mössbauer Parameters of the Used Catalysts

	Mössbauer parameters[a]				
sample	IS (mm s^{-1})	QS (mm s^{-1})	Hhf (kOe)	phase	area (%)
Fe/NCNTs	0.12	0.02	185	χ-Fe_5C_2(I)	68.0
	0.25	0.04	219	χ-Fe_5C_2(II)	16.4
	0.04	0.03	334	α-Fe	9.6
	0.38	1.19	–	Fe^{3+}(spm)[b]	6.0
Fe/t-CNTs	0.10	0.02	187	χ-Fe_5C_2(I)	21.6
	0.14	0.04	219	χ-Fe_5C_2(II)	21.6
	0.22	1.17	–	Fe^{3+}(spm)[b]	56.8

[a]IS = isomer shift, QS = quadrupole splitting, and Hhf = hyperfine field. Isomer shifts are relative to α-Fe. [b]spm = superparamagnetic.

also coincides with the easier reduction and CO adsorption and dissociation for the Fe/NCNTs catalyst than the Fe/t-CNTs catalyst, as reflected in Figure 9a and Figure 8b. The higher content of iron carbides is responsible for the higher catalytic activity for Fe/NCNTs relative to Fe/t-CNTs, with FTYs of 26.5 and 16.2 $\mu mol_{CO}\ g_{Fe}^{-1}\ s^{-1}$, respectively (Table 2). By the way, the obvious α-Fe and trace paramagnetic Fe^{3+} species for the used Fe/NCNTs catalyst are much different from the negligible α-Fe and predominant paramagnetic Fe^{3+} species for the used Fe/t-CNTs catalyst (Figure 9b and Table 3), which also reflects the great contribution of nitrogen participation.

3.4.3. Elimination of the Size Effect. As is known, FTS on group VIII metals is structure-sensitive, and the catalytic activity and selectivity depend on the particle size, especially in the small-size range.[9,38,54−56] For iron catalysts, the influence of particle size is obvious when the particle size is below 6 nm and negligible when the particle size is above 6 nm.[9,38] In this study, the particle sizes for the Fe/NCNTs and Fe/t-CNTs catalysts were ∼8 and ∼10 nm before reaction and increased to ∼12 and ∼15 nm after reaction, respectively (section SI-10 in the Supporting Information). The "large" particle sizes (>6 nm) and "small" size differences for Fe/NCNTs and Fe/t-CNTs both before and after reaction indicate that the particle size is not the crucial factor for their much different catalytic performance. Hence, the support effect due to N-doping is the key factor.

The preceding results indicate that N-doping into CNTs facilitates the immobilization of the iron species, generates basic sites, enhances the CO adsorption and dissociation, inhibits the secondary hydrogenation of lower olefins, promotes the reduction of iron oxide, and accelerates the formation of carbides. These factors favor the design of the catalysts and dramatically improve the performance with higher activity, lower-olefin selectivity, and stability.

dx.doi.org/10.1021/cs400931z | ACS Catal. 2014, 4, 613−621

4. CONCLUSIONS

By means of the anchoring effect and the intrinsic basicity of NCNTs, iron nanoparticles were easily immobilized on NCNTs by simple impregnation without the need for any surface premodification. The so-constructed Fe/NCNTs catalyst with an iron loading of 10 wt % presents superb catalytic performance in FTS to give lower olefins with a high $C_2^=-C_4^=$ selectivity of 46.7%, a high activity (FTY) of 26.5 $\mu mol_{CO}\ g_{Fe}^{-1}\ s^{-1}$, and high stability, which are much better than those of the corresponding Fe/t-CNTs catalyst. Moreover, the high $C_2^=-C_4^=$ selectivity is well-correlated with the intrinsic basicity of the NCNTs support, which enhances the dissociative CO adsorption and promotes the lower-olefin desorption on the derived Fe/NCNTs catalyst. The high activity is attributed to the promoted reduction of iron oxide and accelerated formation of the active χ-Fe_5C_2 phase for the Fe/NCNTs catalyst due to participation of the nitrogen. The high stability mainly results from the anchoring effect and the intrinsic basicity of the NCNTs support, which could prevent the loss of active species and basic sites during operation. All of these merits originate from the participation of the nitrogen, as supported by our experimental characterization. The convenient construction, excellent performance, and rational correlation of properties with structural features for the Fe/NCNTs catalyst suggest a new strategy for the development of advanced FTS catalysts to give lower olefins that is based on the intrinsic basicity of abundant N-doped carbon nanostructures.

■ ASSOCIATED CONTENT

Supporting Information

Characterization of the supports; HRTEM images of the activated Fe/NCNTs; effect of iron loading on CO conversion and $C_2^=-C_4^=$ selectivity; chemical composition of the catalysts; reference data for carbon-supported Fe FTS catalysts to give lower olefins from the literature and this study; Anderson−Schulz−Flory plots for the catalysts in this study; theoretical calculations on the hydrogenation of χ-Fe_5C_2 to CH_4; Raman spectroscopy characterization; TPD profiles for the catalysts; and TEM images and particle size distributions of the Fe/NCNTs and Fe/CNTs catalysts after reaction. This material is available free of charge via the Internet at http://pubs.acs.org.

■ AUTHOR INFORMATION

Corresponding Authors

*E-mail: zhenghu@nju.edu.cn (Z.H.).
*E-mail: wangxzh@nju.edu.cn (X.W.).
*E-mail: xubolian@nju.edu.cn (B.X.).

Notes

The authors declare no competing financial interest.

■ ACKNOWLEDGMENTS

This work was jointly supported by the NNSFC (51232003, 21373108, 21173114, 21203092), the "973" Program (2013CB932902), and the Suzhou Program (ZXG2013025).

■ REFERENCES

(1) Corma, A.; Melo, F. V.; Sauvanaud, L.; Ortega, F. *Catal. Today* **2005**, *107*−*108*, 699−706.
(2) Khodakov, A. Y.; Chu, W.; Fongarland, P. *Chem. Rev.* **2007**, *107*, 1692−1744.
(3) Iglesia, E. *Appl. Catal., A* **1997**, *161*, 59−78.
(4) de Smit, E.; Weckhuysen, B. M. *Chem. Soc. Rev.* **2008**, *37*, 2758−2781.
(5) Zhang, Q. H.; Kang, J. C.; Wang, Y. *ChemCatChem* **2010**, *2*, 1030−1058.
(6) Torres Galvis, H. M.; de Jong, K. P. *ACS Catal.* **2013**, *3*, 2130−2149.
(7) Büssemeier, B.; Frohning, C. D.; Horn, G.; Kluy, W. U.S. Patent 4,564,642, 1986.
(8) Torres Galvis, H. M.; Bitter, J. H.; Khare, C. B.; Ruitenbeek, M.; Dugulan, A. I.; de Jong, K. P. *Science* **2012**, *335*, 835−838.
(9) Torres Galvis, H. M.; Bitter, J. H.; Davidian, T.; Ruitenbeek, M.; Dugulan, A. I.; de Jong, K. P. *J. Am. Chem. Soc.* **2012**, *134*, 16207−16215.
(10) Torres Galvis, H. M.; Koeken, A. C. J.; Bitter, J. H.; Davidian, T.; Ruitenbeek, M.; Dugulan, A. I.; de Jong, K. P. *Catal. Today* **2013**, *215*, 95−102.
(11) Yang, Z. Q.; Guo, S. J.; Pan, X. L.; Wang, J. H.; Bao, X. H. *Energy Environ. Sci.* **2011**, *4*, 4500−4503.
(12) Torres Galvis, H. M.; Koeken, A. C. J.; Bitter, J. H.; Davidian, T.; Ruitenbeek, M.; Dugulan, A. I.; de Jong, K. P. *J. Catal.* **2013**, *303*, 22−30.
(13) Xu, J. D.; Zhu, K. T.; Weng, X. F.; Weng, W. Z.; Huang, C. J.; Wan, H. L. *Catal. Today* **2013**, *215*, 86−94.
(14) Yang, Z. Q.; Pan, X. L.; Wang, J. H.; Bao, X. H. *Catal. Today* **2012**, *186*, 121−127.
(15) Koeken, A. C. J.; Torres Galvis, H. M.; Davidian, T.; Ruitenbeek, M.; de Jong, K. P. *Angew. Chem., Int. Ed.* **2012**, *51*, 7190−7193.
(16) Soled, S.; Iglesia, E.; Fiato, R. A. *Catal. Lett.* **1990**, *7*, 271−280.
(17) Lu, S.; Lonergan, W. W.; Zhu, Y.; Xie, Y.; Chen, J. G. *Appl. Catal., B* **2009**, *91*, 610−618.
(18) Sun, Z.; Sun, B.; Qiao, M.; Wei, J.; Yue, Q.; Wang, C.; Deng, Y.; Kaliaguine, S.; Zhao, D. *J. Am. Chem. Soc.* **2012**, *134*, 17653−17660.
(19) Bao, J.; He, J.; Zhang, Y.; Yoneyama, Y.; Tsubaki, N. *Angew. Chem., Int. Ed.* **2008**, *47*, 353−356.
(20) Shi, L.; Tao, K.; Kawabata, T.; Shimamura, T.; Zhang, X. J.; Tsubaki, N. *ACS Catal.* **2011**, *1*, 1225−1233.
(21) Shou, H.; Ferrari, D.; Barton, D. G.; Jones, C. W.; Davis, R. J. *ACS Catal.* **2012**, *2*, 1408−1416.
(22) Gallegos, N. G.; Alvarez, A. M.; Cagnoli, M. V.; Bengoa, J. F.; Marchetti, S. G.; Mercader, R. C.; Yeramian, A. A. *J. Catal.* **1996**, *161*, 132−142.
(23) Xu, L. Y.; Wang, Q. X.; Xu, Y. D.; Huang, J. S. *Catal. Lett.* **1994**, *24*, 177−185.
(24) Serafin, I.; Kotarba, A.; Grzywa, M.; Sojka, Z.; Bińczycka, H.; Kuśtrowski, P. *J. Catal.* **2006**, *239*, 137−144.
(25) Serp, P.; Corrias, M.; Kalck, P. *Appl. Catal., A* **2003**, *253*, 337−358.
(26) Yue, B.; Ma, Y. W.; Tao, H. S.; Yu, L. S.; Jian, G. Q.; Wang, X. Z.; Wang, X. S.; Lu, Y. N.; Hu, Z. *J. Mater. Chem.* **2008**, *18*, 1747−1750.
(27) Jiang, S. J.; Ma, Y. W.; Jian, G. Q.; Tao, H. S.; Wang, X. Z.; Fan, Y. N.; Lu, Y. N.; Hu, Z.; Chen, Y. *Adv. Mater.* **2009**, *21*, 4953−4956.
(28) Jiang, S.; Zhu, L.; Ma, Y.; Wang, X.; Liu, J.; Zhu, J.; Fan, Y.; Zou, Z.; Hu, Z. *J. Power Sources* **2010**, *195*, 7578−7582.
(29) Su, D. S.; Perathoner, S.; Centi, G. *Chem. Rev.* **2013**, *113*, 5782−5816.
(30) Bitter, J. H.; van Dommele, S.; de Jong, K. P. *Catal. Today* **2010**, *150*, 61−66.
(31) Schulte, H. J.; Graf, B.; Xia, W.; Muhler, M. *ChemCatChem* **2012**, *4*, 350−355.
(32) Chen, H.; Yang, Y.; Hu, Z.; Huo, K. F.; Ma, Y. W.; Chen, Y.; Wang, X. S.; Lu, Y. N. *J. Phys. Chem. B* **2006**, *110*, 16422−16427.
(33) Abbaslou, R. M. M.; Tavasoli, A.; Dalai, A. K. *Appl. Catal., A* **2009**, *355*, 33−41.
(34) Ros, T. G.; van Dillen, A. J.; Geus, J. W.; Koningsberger, D. C. *Chem.—Eur. J.* **2002**, *8*, 1151−1162.

(35) Solhy, A.; Machado, B. F.; Beausoleil, J.; Kihn, Y.; Goncalves, F.; Pereira, M. F. R.; Órfão, J. J. M.; Fiqueiredo, J. L.; Faria, J. L.; Serp, P. *Carbon* **2008**, *46*, 1194−1207.
(36) Moreno-Castilla, C.; López-Ramón, M. V.; Carrasco-Marín, F. *Carbon* **2000**, *38*, 1995−2001.
(37) de Smit, E.; Swart, I.; Creemer, J. F.; Hoveling, G. H.; Gilles, M. K.; Tyliszczak, T.; Kooyman, P. J.; Zandbergen, H. W.; Morin, C.; Weckhuysen, B. M.; de Groot, F. M. F. *Nature* **2008**, *456*, 222−225.
(38) Park, J. Y.; Lee, Y. J.; Khanna, P. K.; Jun, K. W.; Bae, J. W.; Kim, Y. H. *J. Mol. Catal. A: Chem.* **2010**, *323*, 84−90.
(39) Grosvenor, A. P.; Kobe, B. A.; McIntyre, N. S. *Surf. Sci.* **2004**, *572*, 217−227.
(40) Grosvenor, A. P.; Kobe, B. A.; Biesinger, M. C.; McIntyre, N. S. *Surf. Interface Anal.* **2004**, *36*, 1564−1574.
(41) Figueiredo, J. L.; Pereira, M. F. R. *Catal. Today* **2010**, *150*, 2−7.
(42) Kuznetsova, A.; Popova, I.; Yates, J. T., Jr.; Bronikowski, M. J.; Huffman, C. B.; Liu, J.; Smalley, R. E.; Hwu, H. H.; Chen, J. G. G. *J. Am. Chem. Soc.* **2001**, *123*, 10699−10704.
(43) Bahome, M. C.; Jewell, L. L.; Padayachy, K.; Hildebrandt, D.; Glasser, D.; Datye, A. K.; Coville, N. J. *Appl. Catal., A* **2007**, *328*, 243−251.
(44) Huo, C.-F.; Li, Y.-W.; Wang, J. G.; Jiao, H. J. *J. Am. Chem. Soc.* **2009**, *131*, 14713−14721.
(45) Boehm, H. P. *Carbon* **2002**, *40*, 145−149.
(46) Miller, D. G.; Moskovits, M. *J. Phys. Chem.* **1988**, *92*, 6081−6085.
(47) Che, R.; Liang, C.; Shi, H.; Zhou, X.; Yang, X. *Nanotechnology* **2007**, *18*, No. 355705.
(48) Chen, W.; Fan, Z. L.; Pan, X. L.; Bao, X. H. *J. Am. Chem. Soc.* **2008**, *130*, 9414−9419.
(49) Guczi, L.; Stefler, G.; Geszti, O.; Koppány, Z.; Kónya, Z.; Molnár, E.; Urbán, M.; Kiricsi, I. *J. Catal.* **2006**, *244*, 24−32.
(50) Abbaslou, R. M. M.; Tavassoli, A.; Soltan, J.; Dalai, A. K. *Appl. Catal., A* **2009**, *367*, 47−52.
(51) Shroff, M. D.; Kalakkad, D. S.; Coulter, K. E.; Köhler, S. D.; Harrington, M. S.; Jackson, N. B.; Sault, A. G.; Datye, A. K. *J. Catal.* **1995**, *156*, 185−207.
(52) de Smit, E.; Cinquini, F.; Beale, A. M.; Safonova, O. V.; van Beek, W.; Sautet, P.; Weckhuysen, B. M. *J. Am. Chem. Soc.* **2010**, *132*, 14928−14941.
(53) Yang, C.; Zhao, H.; Hou, Y.; Ma, D. *J. Am. Chem. Soc.* **2012**, *134*, 15814−15821.
(54) Boudart, M.; McDonald, M. A. *J. Phys. Chem.* **1984**, *88*, 2185−2195.
(55) Bezemer, G. L.; Bitter, J. H.; Kuipers, H.; Oosterbeek, H.; Holewijn, J. E.; Xu, X. D.; Kapteijn, F.; van Dillen, A. J.; de Jong, K. P. *J. Am. Chem. Soc.* **2006**, *128*, 3956−3964.
(56) Kang, J.; Zhang, S.; Zhang, Q.; Wang, Y. *Angew. Chem., Int. Ed.* **2009**, *48*, 2565−2568.